Dalton Transactions

M–Ge–Si thermolytic molecular precursors and models for germanium-doped transition metal sites on silica

Journal:	*Dalton Transactions*
Manuscript ID	DT-ART-03-2024-000644.R1
Article Type:	Paper
Date Submitted by the Author:	01-Apr-2024
Complete List of Authors:	Dombrowski, James; University of California Berkeley, Chemistry Kalendra, Vidmantas; Vilnius University, Ziegler, Micah; Georgia Institute of Technology, School of Chemical and Biomolecular Engineering; Georgia Institute of Technology, School of Public Policy Lakshmi, K.; Rensselaer Polytechnic Institute, Chemistry and Chemical Biology Bell, Alexis; University of California, Chemical and Biomolecular Engineering Tilley, T.; University of California Berkeley, Chemistry

ARTICLE

M–Ge–Si thermolytic molecular precursors and models for germanium-doped transition metal sites on silica

Received 00th January 20xx,
Accepted 00th January 20xx

DOI: 10.1039/x0xx00000x

James P. Dombrowski,[a,b] Vidmantas Kalendra,[c,d] Micah S. Ziegler,[a,b,e] K. V. Lakshmi,[c] Alexis T. Bell,[b,f] and T. Don Tilley*[a,b]

The synthesis, thermolysis, and surface organometallic chemistry of thermolytic molecular precursors based on a new germanosilicate ligand platform, $-OGe[OSi(O^tBu)_3]_3$, is described. Use of this ligand is demonstrated with preparation of complexes containing the first-row transition metals Cr, Mn, and Fe. The thermolysis and grafting behavior of the synthesized complexes, $Fe\{OGe[OSi(O^tBu)_3]_3\}_2$ (**FeGe**), $Mn\{OGe[OSi(O^tBu)_3]_3\}_2(THF)_2$ (**MnGe**) and $Cr\{OGe[OSi(O^tBu)_3]_3\}_2(THF)_2$ (**CrGe**), were evaluated using a combination of thermogravimetric analysis; nuclear magnetic resonance (NMR), ultraviolet-visible (UV-Vis), and electron paramagnetic resonance (EPR) spectroscopies; and single-crystal X-ray diffraction (XRD). Grafting of the precursors onto SBA-15 mesoporous silica and subsequent calcination in air led to substantial changes in transition metal coordination environments and oxidation states, the implications of which are discussed in the context of low-coordinate and low oxidation state thermolytic molecular precursors.

Introduction

Heterogeneous metal oxide catalysts often possess isolated active sites that consist of one metal center supported by a local coordination sphere comprising surface atoms from the support. These "single-site" catalysts, despite increasing use of the alternative term "single-atom", derive their properties from both the metal (M) and adjacent atoms (E) in the support material, primarily through bonding interactions in M–O–E linkages anchoring the metal to the surface. The M–O–E linkages are commonly involved in generating or stabilizing reactive intermediates and may break and reform to help mediate elementary steps on the reaction pathway (e.g., hydrolysis or alcoholysis and condensation reactions across the oxo bridge); therefore, the chemical identity of the linkages present in a single-site catalyst can have a critical impact on the observed reactivity. Modified single-site catalysts, resulting from incorporation of dopant atoms (E') as promotors, can exhibit improved performance by altering chemical properties of the metal center through introduction of M–O–E' linkages with perturbed electronic effects and bonding chemistry. Thus, control of dopants within a single-site catalyst is of significant interest to the heterogeneous catalysis community.[1–7] The introduction of dopant atoms into the secondary coordination sphere of a metal center poses a synthetic challenge, but is highly desired for the directed, rational assembly of well-defined active sites of enhanced catalytic efficiency.

Interdisciplinary research at the interface of organometallic chemistry and surface science has created the field of *surface organometallic chemistry* (SOMC), involving deposition of well-defined organometallic and coordination complexes onto the surface of a material to generate well-defined and tailored active-sites.[8–15] This laboratory has developed a related methodolgy for construction of well-defined catalytic sites, termed the *thermolytic molecular precursor* (TMP) method.[16–25] This method involves surface

a *Department of Chemistry*
University of California, Berkeley
Berkeley, CA, USA
E-mails: tdtilley@berkeley.edu
b *Chemical Sciences Division*
Lawrence Berkeley National Laboratory
1 Cyclotron Road, Berkeley, CA, USA
c *Department of Chemistry and Chemical Biology*
and
The Baruch '60 Center for Biochemical Solar Energy Research
Rensselaer Polytechnic Institute
Troy, NY 12180, USA
d *Current Address*
Institute of Applied Electrodynamics and Telecommunications
Vilnius University
Saulėtekio av. 9, III bld., Vilnius, LT-10222
e *Current Address*
School of Chemical and Biomolecular Engineering
Georgia Institute of Technology
311 Ferst Drive, NW, Atlanta, GA 30332-0100
and
School of Public Policy
Georgia Institute of Technology
258 4th Street, Atlanta, GA 30332 – 0345
f *Department of Chemical and Biomolecular Engineering*
University of California, Berkeley
201 Gilman Hall, Berkeley, CA, USA

Electronic Supplementary Information (ESI) available: Supporting information for this article includes experimental details, nitrogen porosimetry data and analyses, IR, UV-Vis, supporting EPR, and NMR spectra, and crystallographic data tables. CCDC Deposition Numbers 2332271-2332274 contain the supplementary crystallographic data for for **MnGe**, **HOGe**, **FeGe**, and **CrGe**, sequentially. These data are provided free of charge by the joint Cambridge Crystallographic Data Centre and Fachinformationszentrum Karlsruhe Access Structures service www.ccdc.cam.ac.uk/structures.

attachment of molecular species that are chemically designed to undergo facile, low-temperature elimination reactions to generate stable, inorganic catalytic sites. This immobilization strategy (Scheme 1) usually involves molecular precursors containing *tert*-butoxy groups, which undergo acid-catalyzed eliminations of isobutene to generate single-site catalytic centers possessing M–O–E linkages to the surface.

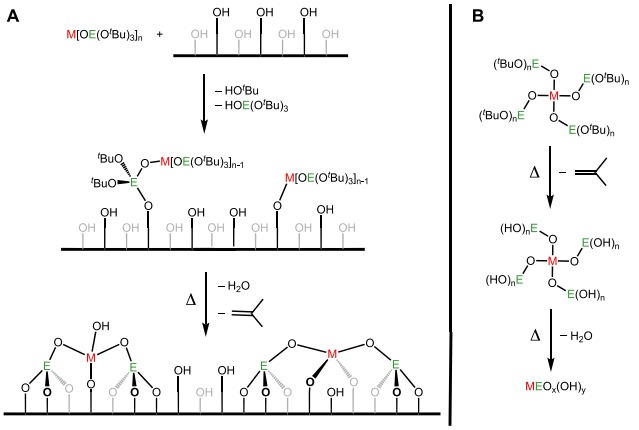

Scheme 1. A) Generic scheme for generation of single-site catalytic sites *via* the TMP method. B) Generic example of TMP precursor transformation to a mixed-element oxide material.

The TMP method is suited for the formation of well-defined surface species as it allows preassembly of active metals and elemental modifiers into an oxidic core of the precursor prior to grafting and thermolysis. This laboratory has illustrated this principle in prior work with, for example, germanium as a chemical modifier.[26,27] Several reports describe enhancements of catalytic activity for oxidation reactions with inclusion of germanium as a modifier into metal-doped silicas or molecular complexes.[26–38] For example, work on tantalum silsesquioxanes revealed enhancements in catalytic activity for liquid-phase epoxidations with the tantalum atoms having oxo-linkages to germanium atoms.[35] Investigation of germanium-doped Ti-SBA15 catalysts generated from a titanium germyloxide precursor, Ti[OGe^{i}Pr$_3$]$_4$, also indicated enhanced activity in liquid-phase epoxidations when compared to germanium-free Ti-SBA15 samples.[26]

The successful deposition of titanium-germoxy sites onto SBA-15 using Ti[OGe^{i}Pr$_3$]$_4$ revealed limitations of the –OGe^{i}Pr$_3$ ligand for TMP applications, presumably because this precursor does not contain Ge–OR alkoxy substituents (e.g., Ge–O^{t}Bu) that can serve as "masked Ge–OH" groups that undergo a clean and facile alkene elimination.[26] Indeed, Ti[OGe^{i}Pr$_3$]$_4$ does not exhibit the low-temperature thermolysis behavior associated with related M–OSi(O^{t}Bu)$_3$ complexes, and instead undergoes sublimation under a nitrogen atmosphere and thermally decomposes only in the presence of an oxidizing atmosphere (air or oxygen). Moreover, calcination of grafted [^{i}Pr$_3$GeO]$_3$Ti-SBA15 samples produced materials that retain a significant amount of carbon as a contaminant. Thus, development of new TMP-compatible ligands for the controlled deposition of metal sites containing M–OGe linkages is an attractive goal.

Previous attempts to access suitable germyloxide TMP precursors have been thwarted by the difficulty in synthesizing the proligand HOGe(O^{t}Bu)$_3$, analogous to the readily prepared, useful silanol HOSi(O^{t}Bu)$_3$.[16–18,26] Thus, attention turned to elaborate and potentially more stable germanium-containing ligand precursors analogous to HOB[OSi(O^{t}Bu)$_3$]$_2$, which can be prepared on a large scale and provides TMP precursors to M–B–Si oxides.[39–41] This finding suggested that incorporation of –OSi(O^{t}Bu)$_3$ groups about germanium could result in new TMP precursors that allow retention of M–O–Ge bonds in the final solid-state material.

This contribution describes the synthesis of HOGe[OSi(O^{t}Bu)$_3$]$_3$ and its use in preparing M(II) complexes (where, M = Fe, Mn, Cr) containing the –OGe[OSi(O^{t}Bu)$_3$]$_3$ ligand. The thermolysis behavior of these complexes was found to be similar to that of analogous TMP precursors based on –OSi(O^{t}Bu)$_3$ ligands. The grafting behavior of these complexes onto SBA-15 mesoporous silica and the thermolyses of surface-grafted complexes during calcination in oxygen are reported herein. Characterization of the calcined samples suggests the formation of oxidized, isolated metal centers with substantial change in coordination geometry relative to that of the precursors. For some samples a distribution of isolated sites were obtained after thermolysis of grafted-precursors, as indicated by electron paramagnetic resonance (EPR) spectroscopy.

This work identifies a new platform ligand from which germanium-containing materials are expected to be generated by similar TMP methodologies as have been previously performed using precursors based on the –OSi(O^{t}Bu)$_3$ ligand, namely direct precursor thermolysis,[19,42–44] grafting followed by thermolysis,[20–24,45–47] and co-thermolysis.[42,48] This work describes in detail the thermolysis and grafting properties of the new ligand, in support of its use to generate TMP precursors. Of specific future interest is the synthesis of transition metal precursors for which Ge-based promotor effects on metal-based catalysis have been identified, especially the titanium and tantalum systems described above, and work towards this goal has begun.

Results

The synthesis of HOGe[OSi(O^{t}Bu)$_3$]$_3$ (**HOGe**) was achieved by simple salt metathesis and hydrolysis reactions (Scheme 2). Germanium tetrachloride was treated with ~3.2 equivalents of sodium tris(*tert*-butoxy)silanolate in THF with immediate formation of a white precipitate — presumably sodium chloride. After 24 h, the suspension was concentrated to dryness *in vacuo* and the solid residue was extracted with pentane and then filtered. The resulting solution was again concentrated to dryness *in vacuo* to give crude ClGe[OSi(O^{t}Bu)$_3$]$_3$ (**ClGe**) as a crystalline powder, which was recrystallized from THF at –30 °C. Treatment of **ClGe** with 1.1 equivalents of pyridine and ~13 equivalents of water in toluene at 20 °C for 6 h led to formation of a white precipitate and a colorless

solution. Concentration of the reaction mixture to dryness followed by extraction of the white residue with pentane gave a translucent suspension. Filtration of the suspension gave a colorless solution that was subsequently concentrated *in vacuo* to give a white solid. The ^{1}H NMR spectrum (benzene-d_6) of this solid displayed a small singlet at 3.81 ppm as well as a signal at 1.50 ppm, corresponding to the final product. A significant amount of tris(tri-*tert*-butoxy)silanol (**HOSi**) was also observed and was presumably formed by competitive hydrolysis of the Ge–O–Si linkage. Complete conversion of **ClGe** to HOGe[OSi(O^{t}Bu)$_3$]$_3$ (**HOGe**) and **HOSi** was readily confirmed by ^{13}C{^{1}H} NMR spectroscopy. No other products were observed by either ^{1}H or ^{13}C{^{1}H} NMR spectroscopy suggesting that other germanium-based products generated by elimination of **HOSi** decomposed further to germanium oxide or are insoluble in pentane. Conveniently, **HOSi** can be removed from the crude **HOGe** by its sublimation *in vacuo* at 70 °C

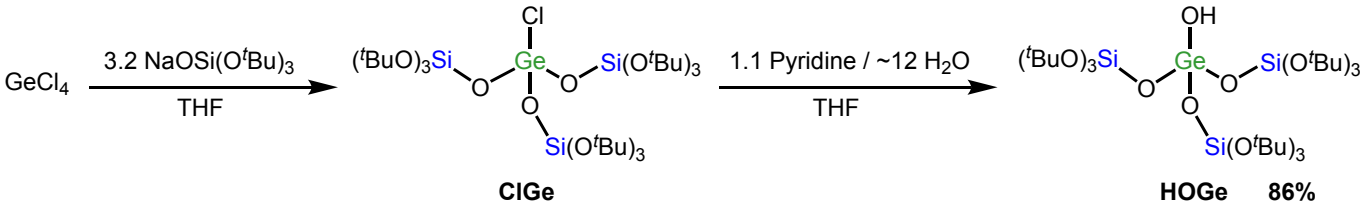

Scheme 2. Generation of **ClGe** by salt metathesis between sodium tris(*tert*-butoxy)silanolate and germanium tetrachloride and synthesis of **HOGe** *via* hydrolysis of **ClGe**.

Single crystals of **HOGe** were grown from a pentane solution at –30 °C and used for single-crystal X-ray diffraction (XRD) to determine the solid-state structure. Despite structural disorder the connectivity of **HOGe** is confirmed, as well as the presence of a tetrahedrally-coordinated germanium center bonded to three tris(tert-butoxy)siloxide ligands and a terminal hydroxide (Scheme 2).

Given the extreme steric bulk of **HOGe**, M(II) derivatives were targeted in hopes of generating simple compounds with only germoxy ligands. Treatment of [FeMes$_2$]$_2$, Mn[N(SiMe$_3$)$_2$]$_2$(THF)$_2$, and Cr[N(SiMe$_3$)$_2$]$_2$(THF)$_2$ in pentane (Mn or Fe) or THF (Cr) with two equivalents of **HOGe** led to the formation of Fe{OGe[OSi(O^{t}Bu)$_3$]$_3$}$_2$, Mn{OGe[OSi(O^{t}Bu)$_3$]$_3$}$_2$(THF)$_2$, and Cr{OGe[OSi(O^{t}Bu)$_3$]$_3$}$_2$(THF)$_2$. These compositions were confirmed by elemental analysis, and the complexes were characterized by single-crystal XRD and Fourier-transform infrared spectroscopy (FTIR) (Scheme 3 and ESI).

ARTICLE

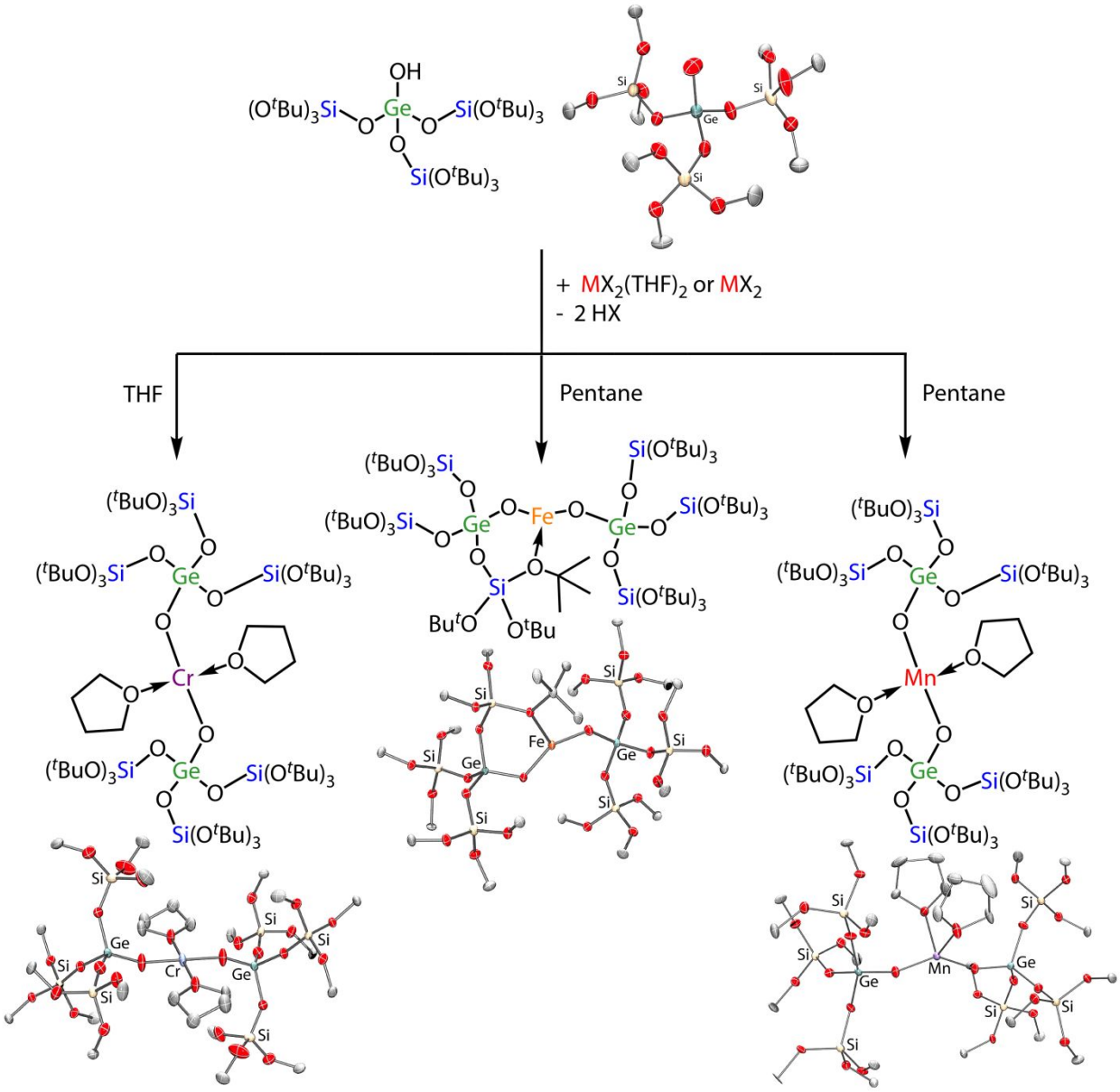

Scheme 3. Synthesis of first-row transition metal germyloxides **CrGe**, **MnGe**, and **FeGe** from **HOGe** by protonolysis. Ellipsoids shown at 50% probability. *Tert*-butyl groups truncated to single carbon atoms for clarity. Co-crystallized solvent excluded.

Single crystals suitable for X-ray diffraction studies of **FeGe** and **MnGe** were grown from pentane solutions at –30 °C while crystals of **CrGe** were grown from THF at the same temperature. While the collection of diffraction data for MnGe was only 87% complete out to 25 º, it is sufficiently complete to identify connectivity. The crystal structures of **MnGe** and **CrGe** indicate pseudo-tetrahedral and square planar geometries around each transition metal center; respectively, with two THF molecules completing the coordination sphere. In **FeGe**, a three-coordinate metal center is formed through ligation of two germoxy ligands and Lewis acid-base coordination of an oxygen atom in one *tert*-butoxide group to the iron atom.

Fourier-transform infrared spectroscopy (FTIR) of **CrGe**, **FeGe**, and **MnGe** showed new vibrational modes between 800 and 1000 cm^{-1} not observed for **HOGe** and near those previously reported for M–O–Ge linkages (Figure S1).[49–51] Two modes located at ~ 875 cm^{-1} (**FeGe**, 877; **MnGe**, 874; **CrGe**, 871) and ~ 845 cm^{-1} (**FeGe**, 843; **MnGe**, 850; **CrGe**, 848) are tentatively assigned to M–O–Ge vibrational modes. The presence of these modes in the **FeGe** IR spectrum suggests they are not due to coordinated THF which is known to display vibrational modes around ~910 and ~865 cm^{-1}.[52]

Thermolysis and grafting studies of HOGe, FeGe, MnGe, and CrGe

Thermogravimetric analysis (TGA) was performed on **FeGe**, **MnGe**, **CrGe,** and **HOGe** to evaluate their thermolytic behavior under a non-oxidizing nitrogen atmosphere (Figure 1). Analogous to tris(tri-*tert*-butoxy)silanol and the boronous acid $HOB[OSi(O^tBu)_3]_2$, **HOGe** sublimes under nitrogen, with onset of the sublimation event at approximately 200 °C.[41,53] The complexes **FeGe**, **MnGe**, and **CrGe**, however, exhibit thermal degradation behavior that is similar to that of other TMP molecular precursors with onset of primary mass-loss events at approximately 150, 180, and 200 °C, respectively. Some initial mass loss is observed prior to 150 °C, which may be attributed to either loss of bound THF/water or partial decomposition. Samples were transferred at liquid nitrogen temperatures to a sample holder blanketed by a flow of nitrogen; however, the possibility of partial oxidation or hydrolysis of the sample during the brief exposure to ambient atmosphere cannot be excluded. It should be noted that measurements indicating somewhat lower than expected residual masses were correlated with observable mass losses prior to 150 °C. Regardless, the residual masses after treatment to 500 °C are largely consistent with loss of all organic fragments and condensation of the hydroxyl groups formed upon decomposition of the *tert*-butoxide groups to isobutene.[19]

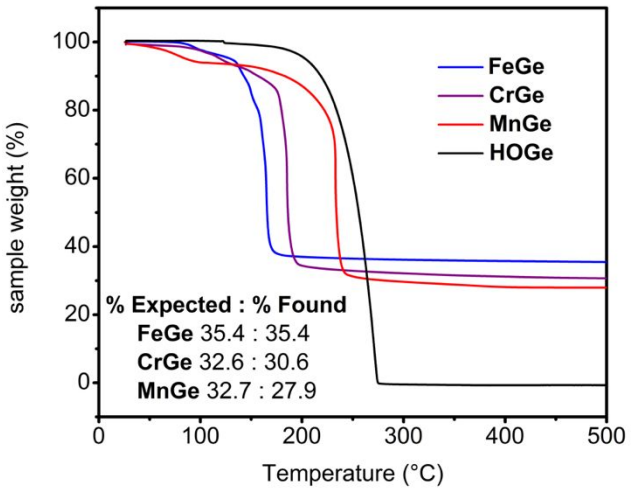

Figure 1. Thermogravimetric analysis of **FeGe**, **CrGe**, **MnGe**, and **HOGe**. % Expected calculated for $MGe_2Si_6O_{14}$.

The initial products of thermal degradation were identified by NMR spectroscopy. The volatile elimination products generated upon thermolysis of **MnGe**, **FeGe,** and **CrGe** at 250 ºC for 30 minutes were collected by vacuum transfer onto benzene-d_6 containing ferrocene as an internal standard. ^{1}H NMR spectroscopy indicated formation of isobutene, *tert*-butanol and water as the primary volatile products with THF also observed for **MnGe** and **CrGe** (Figure S11-S13). Quantification of the products indicated that the collected volatile material accounted for 53% of the THF and 43% of *tert*-butoxide groups from **MnGe**, ~100% of the THF and 53% of *tert*-butoxide groups from **CrGe** and 28% of the *tert*-butoxide groups from **FeGe**. It can therefore be concluded that the thermolysis behavior of the metal precursors is analogous to that of tris(tri-*tert*-butoxy)silanolate-based complexes previously developed for use in the TMP method.[16–19]

Especially given the presence of potentially hydrolysable Ge–OSi linkages in **HOGe**, it's stability against hydrolysis and protonolysis by weakly-acidic silanols present on a silica surface was investigated. Unlike **HOSi** and $HOGe^iPr_3$, **HOGe** was found to be susceptible to hydrolysis. However, when **HOGe** was treated with 10 equivalents of H_2O in benzene-d_6, **HOSi** was not observed as the major soluble product by ^{1}H NMR spectroscopy. Instead, a broad resonance appeared near 5 ppm vs $Si(CH_3)_4$ (Figure S14). Concurrently, deposition of a solid precipitate was observed in the NMR tube. Having identified that **HOGe** is unstable to water exposure, its stability to surface silanols on SBA-15 was similarly investigated. No soluble elimination products were observed by ^{1}H NMR spectroscopy after two days of exposure of **HOGe** to a suspension of SBA-15 in benzene-d_6 at 20 ºC. However, *tert*-butanol has been observed as an elimination product from grafting of metal precursors based on **–OSi** even though **HOSi** is stable against ambient hydrolysis.[20]

Grafting of **FeGe**, **CrGe**, and **MnGe** onto SBA-15 silica was performed in the same manner as previously described for many other TMP precursors.[16–18,20–23,26,54,55] Complex grafting behavior was observed, with both silanol and germanol elimination products identified by ^{1}H NMR spectroscopy. These elimination products ranged from ~30–80% of available **–OGe** and ~5-30% of available **–OSi** depending on the conditions. For continued study, significant quantities of samples prepared by loading **FeGe**, **CrGe**, and **MnGe** onto SBA-15, denoted **FeGe-SBA15**, **CrGe-SBA15**, and **MnGe-SBA15**, were obtained with a nominal target of ~1.5 wt% metal content (See ESI). The filtrates from washing of the samples were collected and concentrated to dryness *in vacuo* to give white residues of elimination products, which were identified and quantified by ^{1}H NMR spectroscopy in the presence of a ferrocene internal standard. Rather than a ~6:1 molar ratio of germanol to silanol, which was observed when grafting with excess precursor in small scale tests using J-Young tubes (Figures S15-S17), a molar ratio of ~ 3:1 germanol to silanol was observed in the large scale experiments. For **MnGe**, 0.97 equivalents of **HOGe** per metal center were eliminated, along with 5% of the available silanol groups. Likewise, for **FeGe**, 0.84 equivalents of **HOGe** were eliminated along with 5% of the silanol. These results were corroborated by elemental analysis of **FeGe-SBA15** and **MnGe-SBA15** samples after calcination, with observation of a Fe:Ge ratio of 0.88:1 and a Mn:Ge ratio of 1.01:1, indicating that approximately one

germanium atom was deposited along with each transition metal center.

As-grafted **MGe-SBA15** (M = Fe, Cr) materials were calcined under an oxygen atmosphere at 300 °C for 3 h to generate **MGe-SBA15$_{calc}$** samples. **MnGe-SBA15** required calcination at the higher temperature of 350 °C to generate carbon-free **MnGe-SBA15$_{calc}$**. C–H stretching modes were absent in Fourier-transform infrared spectroscopy (FTIR) spectra of the calcined samples, suggesting near-complete elimination of the *tert*-butoxy fragments from the surface-bound complexes (Figure S2).

Following calcination, nitrogen porosimetry studies on the **MGe-SBA15$_{calc}$** samples revealed only modest loss of surface area, and preserved pore radii of ~2.9 nm. Type IV isotherms with H1 hysteresis loops at high relative P/P_o values are observed as expected for well-ordered mesoporous SBA-15 materials (Figure S3).[56,57] This indicates that the synthetic procedure does not significantly change the porosity and physical characteristics of the support material.

Diffuse-reflectance ultraviolet-visible spectroscopy (DRUV-Vis) of MGe-SBA-15$_{calc}$ samples

Upon calcination, significant changes in the colors of all samples were observed and subsequently characterized through diffuse reflectance UV-visible spectroscopy. **FeGe-SBA15** changed from white to yellow, **MnGe-SBA15** turned from white to pink, and pale bluish-purple **CrGe-SBA15** changed to bright yellow. UV-vis spectra provided evidence for the presence of isolated surface sites in all samples (Figure S4). For **FeGe-SBA15$_{calc}$**, the spectrum displays a single peak at 252 nm which is consistent with isolated tetrahedral iron(III) centers and the lack of an additional signal around 330 nm suggests that there are no domains of iron oxide of significant size.[22,23] The UV-vis spectrum of **MnGe-SBA15$_{calc}$** exhibits two bands at 235 nm and 470 nm with the former previously attributed to a O→Mn LMCT band for Mn(III)O_4 tetrahedra in a framework position and the latter proposed to be due to defect or surface Mn(II) or Mn(III) sites in several reports of Mn-based silica materials.[58–65] Alternatively, Meng *et al*. suggest that the latter peak is consistent with d→d transitions of Mn(II) in an octahedral oxygen-donor environment as well as both ligand to metal and d→d transitions of Mn(III) in a tetrahedral oxygen-donor environment.[66] For **CrGe-SBA15$_{calc}$**, bands consistent with the presence of chromate and/or dichromate species are found at 235, 320, 420 nm while the absorption at 607 nm can be attributed to surface Cr(III) sites.[67] The lack of signals at 714 nm suggests the absence of large chromia domains.[67]

Electron Paramagnetic Resonance Spectroscopy of MGe Precursors and Materials

The precursors, grafted materials, and calcined materials were characterized using both parallel- and perpendicular-mode electron paramagnetic resonance (EPR) spectroscopy. Spectroscopic assignment identified the structural and electronic changes to the metal center following each of these synthetic steps (Figure 2).

ARTICLE

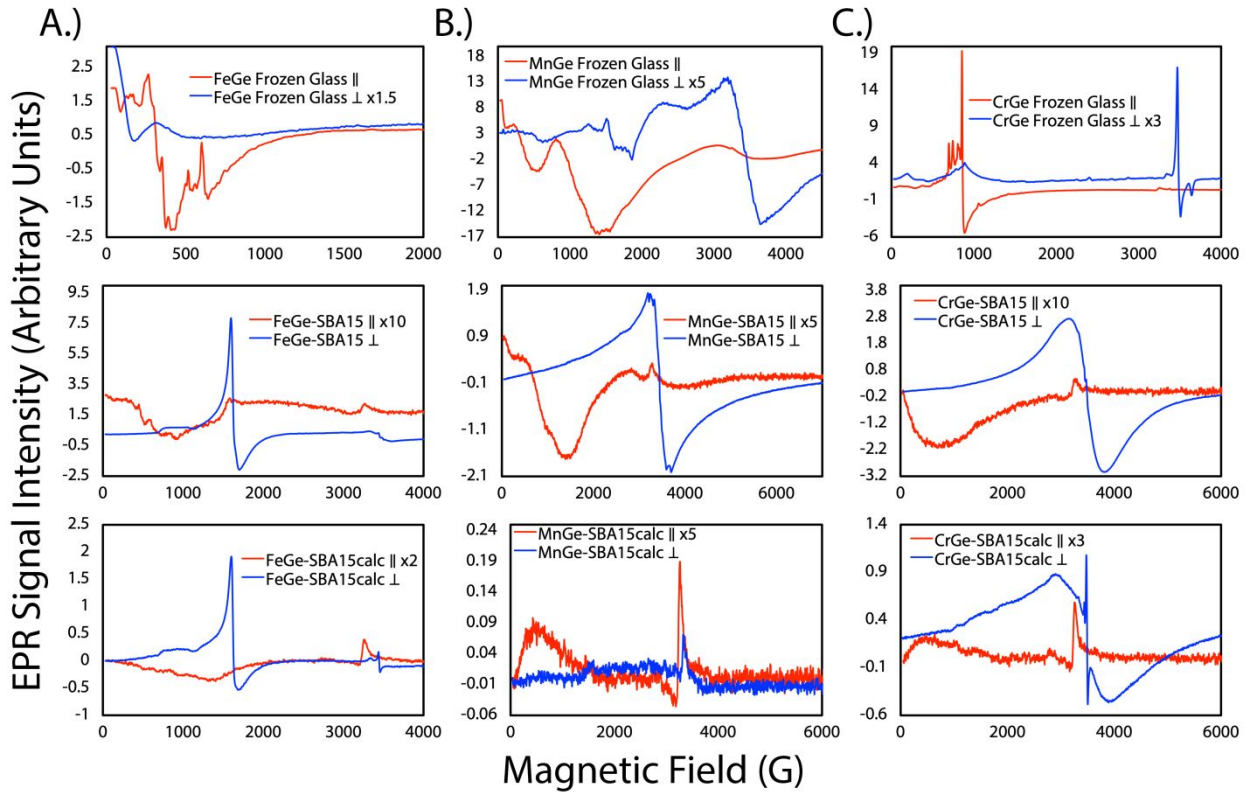

Figure 2. Top to bottom: Parallel (||)- and perpendicular (⊥)-mode EPR spectra of A.) **FeGe**, B.) **MnGe**, and C.) **CrGe** frozen glass (pentane for **FeGe** and **MnGe**, THF for **CrGe**), as-grafted samples on SBA-15, and calcined samples on SBA-15. xN indicates multipliers applied to the raw data to facilitate visualization. All spectra were measured at 10 °K.

Parallel-mode EPR spectra of the **FeGe** precursor in frozen pentane at 10 K indicated the presence of an isolated monomeric high-spin Fe(II) center with an integer electron spin, S, of 2 ($3d^6$ electron configuration) — a species unobservable by conventional perpendicular-mode EPR spectroscopy.[68] When the zero-field splittings for non-Kramers (integer spin) systems are close to the microwave frequency at X-band (~ 9.6 GHz), which is the case for Fe(II), the selection rule for transitions within the integer-spin manifold can be met by parallel-mode EPR spectroscopy.[68–73] **FeGe** in solution exhibits strong parallel-mode EPR resonances at g ≈ 15.65 and 10.49 that arise from a monomeric high-spin S = 2 Fe(II) center (Figure 2 and S5).[70,74] A lack of perpendicular-mode EPR resonances beyond very trace signals at g values of ≈ 4 and 2.0 indicates that the **FeGe** precursor does not contain Fe(III) impurities in solution (Figure S5).

Following grafting of the **FeGe** precursor onto SBA-15, the resulting **FeGe-SBA15** samples display resonances at g ≈ 4 and 2 in the perpendicular-mode EPR spectra (Figure 2). The g ≈ 4 signal is attributed to rhombically-distorted tetrahedral Fe(III) centers and the g = 2.0 signal is associated with octahedral or tetrahedral Fe(III) centers.[75–77] The presence of these signals suggests some oxidation during grafting. This result was also observed in prior work from this laboratory on grafting a related iron (II) silyloxide complex onto SBA-15.[23] It is important to note that the spectral features in the g ≈ 5–40 region observed in the parallel-mode EPR spectra of the precursors persist in the as-grafted **FeGe-SBA15** sample suggesting preservation of Fe(II) centers. Calcination of this sample in air and dehydration under vacuum generated **FeGe-SBA15$_{calc}$**, which displays more prominent perpendicular-mode EPR signals at g ≈ 4 and g ≈ 2. There are no signals visible at g ≈ 2.2–2.5, suggesting the absence of large iron oxide nanoparticles.[22,23,75,78] This is consistent with the UV-Vis spectra described above. Signals from Fe(II) centers in the corresponding parallel-mode EPR spectra remain after calcination, which indicates a distribution of oxidation states in the

final materials even after treatment in oxygen at elevated temperatures.

The perpendicular-mode EPR spectrum of a frozen pentane glass containing **MnGe** displays a major resonance at g ≈ 2 with wings at g ≈ 4.18, 3.01, and 1.49 (Figure 2 and S6). The resonance at g ≈ 2 arises from the –1/2 to 1/2 Kramers doublet of the S = 5/2 spin manifold for a Mn(II) center ($3d^5$ electron configuration). The weak, broad signals that are observed in the wings of the –1/2 to 1/2 transition indicate additional transitions due to small zero-field splittings typical of isolated tetrahedral Mn(II) centers.[79–83] The parallel mode EPR spectrum displays signals below 2000 G reflecting those of the perpendicular mode wings.

The perpendicular- and parallel-mode EPR spectra of **MnGe** as-grafted on SBA15 (**MnGe-SBA15)** and calcined (**MnGe-SBA15$_{calc}$**) were also investigated (Figure 2). Similar perpendicular-mode and parallel-mode signals are observed in **MnGe-SBA15** as found for **MnGe** in pentane glass with a major signal at g ≈ 2 in perpendicular mode and signals below 2000 G in the parallel mode (Figure 2). Calcination and dehydration leads to loss of the majority of the signal in **MnGe-SBA15$_{calc}$**. This is either due to an increase in the zero-field splittings and line-broadening upon calcination and dehydration of **MnGe-SBA15** or the generation of "EPR-silent" Mn(III) species.[84] As previously observed with related manganese-containing silicates, a **MnGe-SBA15$_{calc}$** sample exposed to ambient moisture showed a ½ Kramer's sextet at g ≈ 2.0 attributed to Mn(II) in an isotropic environment, perhaps generated by coordination of water to form an octahedral species which is perturbed upon dehydration (Figure S7 and S8).[60–62,64,85,86] The weakening of perpendicular-mode signals for **MnGe**-based materials is accompanied by a loss of the corresponding signals in the parallel-mode spectrum.

It is highly unusual to observe resonances in perpendicular- or parallel-mode EPR spectra for Cr(II) species at the X-band EPR frequency of ~ 9.6 GHz. Therefore, the strong, distinct resonances observed in spectra measured for **CrGe** as a frozen glass of THF were a surprising result. An isolated monomeric high-spin Cr(II) center has an integer electron spin, S, of 2 ($3d^4$ electron configuration) which is a non-Kramers system. Most studies in the literature have required high-frequency EPR spectroscopy to probe the low-energy electronic structure of non-Kramers systems, such as Cr(II).[84,87,88] Comprehensive high-frequency EPR measurements on Cr(II) in a frozen aqueous solution have found that the D tensor of the $[Cr(H_2O)_6]^{2+}$ species is axially symmetric with a regular tetragonal CrO_6 framework.[89,90] Moreover, a multi-frequency EPR study on $[Cr(D_2O)_6]^{2+}$ in Tutton's salts has demonstrated that while resonances from Cr(II) rapidly broaden above 200 K, the perpendicular mode EPR resonances can be observed at 7 K.[91] Herein, the zero-field splittings for non-Kramers Cr(II) in the **CrGe** precursor is demonstrated to be near axial and close to the microwave frequency at X-band (~ 9.6 GHz), so the selection rule for transitions within the integer-spin manifold can be met by both perpendicular- and parallel-mode EPR spectroscopy. It should be noted, however, that the perpendicular modes observed are consistent with prior reports on Cr(III) species which suggests possible partial oxidation.[92–95] In the parallel mode, the **CrGe** precursor in solution exhibits strong EPR resonances at g ≈ 9.61, 9.0, and 7.73 that arise from a monomeric high-spin S = 2 Cr(II) center (Figure 2 and S9). Similar to previous observations with Fe(II) species, it is expected that the g values of these parallel-mode resonances depend on the zero-field splitting parameters.[70,74]

Upon grafting the **CrGe** precursor onto SBA-15 and after calcination in air, the resulting **CrGe-SBA15** and **CrGe-SBA15$_{calc}$** samples display weak resonances in both the perpendicular- and parallel-mode EPR spectra (Figure 2). This is likely due to differences in the zero-field splittings of the Cr(II) center in **CrGe-SBA15** that makes it harder to detect at X-band EPR frequency. The use of X-band EPR spectroscopy provides a limited window to observe the multitude of transitions that could arise from a high-spin non-Kramers Cr(II) species. The zero-field splittings are within this window in the case of the Cr(II) center in the **CrGe** precursor however immobilization leads to differences in these parameters that contribute to a loss of spectral intensity from any Cr(II) species present. In **CrGe-SBA15$_{calc}$** formation of significant diamagnetic Cr(VI) species, as indicated by UV-Vis spectroscopy, would contribute to a loss of signal.

Discussion

The germanium-silicon compound **HOGe** allows for the generation of new TMP precursor candidates exhibiting thermal degradation behavior that should make them amenable to applications in materials chemistry and catalysis. While thermolysis and calcination in oxygen were performed for bulk materials reported herein, the TMP method has also been used to generate supported low-oxidation state metal centers when thermolysis was performed under non-oxidizing conditions.[24,45] Therefore, TGA results indicating clean thermal decomposition of **HOGe**-based complexes under nitrogen suggests that germanium-doped metal sites in low oxidation states are accessible from these complexes provided oxidizing environments are avoided. This laboratory has also extensively explored the generation of xerogel silica materials by decomposition of TMP precursors in solution under vacuum or nitrogen.[19,40,42–44,48] These synthesis protocols applied to **HOGe**-based precursors should allow for the formation of M–Ge–Si quaternary metal oxides in a similar fashion to previously reported M-B-Si materials.[40]

The stability of the ligand precursor **HOGe** and the grafting behavior of metal complexes containing the **–OGe** ligand differ from the behavior of **HOSi** or **–OSi** based precursors when applied in the the TMP method. **HOGe** differs from **HOSi** in its hydrolytic stability; while **HOSi** is stable to water, **HOGe** reacts to form solid precipitates and soluble species, although the exact identity of these products has not been determined. Additionally, complex grafting behavior is observed for **FeGe** and **MnGe**, where elimination of both germanol and silanol is observed but the ratio and amounts of elimination products vary with the experimental conditions of grafting. It should be noted that *tert*-butanol was not observed as a side product in these experiments, although this alcohol has been observed as an

elimination product during grafting of **–OSi** based precursors in prior literature.[20]

The use of preformed M–O–Ge linkages in the precursor was meant to generate species that preserve these linkages once the precursor was grafted to the surface of silica. While the presence of both transition metals and germanium were confirmed by elemental analysis in the final calcined materials, it was not possible to definitively assign the presence of M–O–Ge linkages on the silica surface. The complexes reported here are in the M(II) oxidation state, and correspondingly contain only two X-type ligands and are sensitive to both expansion of their coordination sphere and oxidation to higher states. UV-Vis spectroscopy provides evidence that upon calcination, primarily tetrahedral sites are generated for all materials. Unlike the previously studied precursor $Ti[OGe^{i}Pr_3]_4$, which is already in the expected geometry and oxidation state for the eventual surface site, the surface species of MGe-$SBA15_{calc}$ likely arise from the unsually low coordination numbers of the precursors and significant coordinative expansion that occurs upon calcination and/or grafting.

Through EPR spectroscopy, it was possible to track the coordination geometry and oxidation states of the precursor molecules in greater detail from the solution species to grafted complexes to calcined surface sites. For **FeGe**, partial oxidation occurred upon grafting monomeric Fe(II) centers in solution to a mixture of Fe(II) and tetrahedral plus possibly octahedral Fe(III) centers on the surface. This geometric change upon grafting may be attributed to the expected expansion of the coordination sphere relative to that of the precursor, through interaction with silanols and siloxane groups on the silica surface. Subsequent calcination led to additional formation of Fe(III) centers; however, signals for monomeric Fe(II) species remained and no evidence for polymeric iron oxide species was observed. Somewhat in contrast, **MnGe** was observed to largely preserve monomeric tetrahedral Mn(II) centers upon grafting, and evidence for significant change in the manganese local environment was only observable by EPR after calcination. Following calcination, loss of EPR signal intensity likely occurs by generation of diamagnetic tetrahedral Mn(III) centers, which is consistent with UV-vis spectroscopy, but the presence of hydrated Mn(II) and Mn(III) species is supported by EPR spectroscopy of calcined samples that did not undergo dehydration for glovebox storage. The precursor complex **CrGe** was notably observed as a monomeric, high-spin Cr(II) center in solution, albeit with possible Cr (III) contamination; however, the signal was substantially lost upon grafting, making identification of specific Cr(II) or Cr(III) environments challenging. In this case, UV-vis spectroscopy of the calcined samples suggests oxidation of chromium centers to the diamagnetic Cr(VI) oxidation state, contributing to the loss of signal by EPR spectroscopy. In general, all metal centers undergo significant structural and oxidative changes through the process of precursor grafting and calcination.

As significant structural changes were observed in grafting and calcining the low-coordinate, low oxidation state transition metal complexes reported herein, future efforts will involve immobilzation protocols that allow greater control over coordination number and oxidation state. In this respect, promising targets are single-site titanium(IV) and tantalum(V) species, which have formed the basis for numerous catalytic oxidation studies and may display enhanced activity in the presence of second-sphere germanium atoms. Initial efforts to synthesize fully-substituted precursors with –OGe ligands from readily available metal starting materials have been unsuccessful. This difficulty is attributed to the steric bulk of **HOGe** and the challenge of assembling 4 or 5 such ligands around a metal center.

Conclusions

This work introduces a readily prepared ligand precursor (**HOGe**) that allows low-temperature thermal conversion to metal-containing materials that incorporate -$OGe(OSi)_3$ units. Preliminary studies show that **HOGe** may be used to synthesize Cr, Mn, and Fe derivatives *via* straightforward protonolysis reactions. Significantly, the $M–OGe[OSi(O^tBu)_3]_3$ complexes reported here transform under mild conditions as TMP precursors to eliminate isobutene, *tert*-butanol, THF, and water in a manner previously established for various efficient precursors based on $–OSi(O^tBu)_3$ ligands. These studies also indicate that **HOGe**-based precursors, like those derived from $–OSi(O^tBu)_3$, can serve as effective reagents for introduction of single-site metal centers on an oxide surface. In the cases described here involving Mn, Fe, and Cr, the metal centers of interest undergo redox processes during thermal conversions in oxygen and air, as might be expected for these metals. Future efforts will probe the utility of early transition metal $M–OGe[OSi(O^tBu)_3]_3$ (M = Ti, Ta, V, etc.) complexes involving persistent, high oxidation states known to function in single-site catalytic centers.[46,47]

Author Contributions

All authors contributed to the writing and review of the manuscript. JPD co-designed the study, performed all syntheses, grafting experiments, NMR, IR, and XRD experiments, and was primary writer of the manuscript and supporting. VK and KVL performed EPR studies and analyses. MSZ assisted with solving of crystal structures. ATB and TDT advised JPD and co-designed the study.

Conflicts of interest

There are no conflicts to declare.

Acknowledgements

This work was primarily supported by the Director, Office of Energy Research, Office of Basic Energy Sciences, Chemical Sciences Division, of the U.S. Department of Energy (DOE) under Contract DE-AC02-05CH11231 (T.D.T., A.T.B.) and DE-FG02-07ER15903 (K.V.L.). We acknowledge the National Institutes of Health (NIH) for funding the UC Berkeley CheXray X-ray crystallographic facility under grant no. S10-RR027172 and the UC Berkeley College of Chemistry NMR

facility under grant nos. SRR023679A and 1S10RR016634-01. M.S.Z. was supported by a National Science Foundation (NSF) Graduate Research Fellowship (grant no.: DGE 1106400) and a Philomathia Graduate Fellowship in the Environmental Sciences.

Notes and references

1 T. Tabakova, M. Manzoli, F. Vindigni, V. Idakiev and F. Boccuzzi, *J. Phys. Chem. A*, 2010, **114**, 3909–3915.
2 J. Ke, J.-W. Xiao, W. Zhu, H. Liu, R. Si, Y.-W. Zhang and C.-H. Yan, *J. Am. Chem. Soc.*, 2013, **135**, 15191–15200.
3 X. Yang, J. Han, Z. Du, H. Yuan, F. Jin and Y. Wu, *Catal. Commun.*, 2010, **11**, 643–646.
4 B. Yang, R. Burch, C. Hardacre, G. Headdock and P. Hu, *ACS Catal.*, 2012, **2**, 1027–1032.
5 J. M. Thomas, R. Raja and D. W. Lewis, *Angew. Chem. Int. Ed.*, 2005, **44**, 6456–6482.
6 A. Okamoto, R. Nakamura, H. Osawa and K. Hashimoto, *Langmuir*, 2008, **24**, 7011–7017.
7 H. Han and H. Frei, *J. Phys. Chem. C*, 2008, **112**, 8391–8399.
8 P. Sautet and F. Delbecq, *Chem. Rev.*, 2010, **110**, 1788–1806.
9 J. D. A. Pelletier and J.-M. Basset, *Acc. Chem. Res.*, 2016, **49**, 664–677.
10 C. Copéret, M. Chabanas, R. Petroff Saint-Arroman and J.-M. Basset, *Angew. Chem. Int. Ed.*, 2003, **42**, 156–181.
11 P. Serna and B. C. Gates, *Acc. Chem. Res.*, 2014, **47**, 2612–2620.
12 R. Anwander, *Chem. Mater.*, 2001, **13**, 4419–4438.
13 C. Copéret, A. Comas-Vives, M. P. Conley, D. P. Estes, A. Fedorov, V. Mougel, H. Nagae, F. Núñez-Zarur and P. A. Zhizhko, *Chem. Rev.*, 2016, **116**, 323–421.
14 J. M. Basset and A. Choplin, *J. Mol. Catal.*, 1983, **21**, 95–108.
15 J.-P. Candy, B. Didillon, E. L. Smith, T. B. Shay and J.-M. Basset, *J. Mol. Catal.*, 1994, **86**, 179–204.
16 K. L. Fujdala, R. L. Brutchey and T. D. Tilley, in *Surface and Interfacial Organometallic Chemistry and Catalysis*, eds. C. Copéret and B. Chaudret, Springer Berlin Heidelberg, 2005, pp. 69–115.
17 T. D. Tilley, *J. Mol. Catal. Chem.*, 2002, **182**, 17–24.
18 K. L. Fujdala and T. D. Tilley, *J. Catal.*, 2003, **216**, 265–275.
19 K. W. Terry, C. G. Lugmair and T. D. Tilley, *J. Am. Chem. Soc.*, 1997, **119**, 9745–9756.
20 J. Jarupatrakorn and T. D. Tilley, *J. Am. Chem. Soc.*, 2002, **124**, 8380–8388.
21 D. A. Ruddy and T. D. Tilley, *J Am Chem Soc*, 2008, **130**, 11088–11096.
22 C. Nozaki, C. G. Lugmair, A. T. Bell and T. D. Tilley, *J. Am. Chem. Soc.*, 2002, **124**, 13194–13203.
23 A. W. Holland, G. Li, A. M. Shahin, G. J. Long, A. T. Bell and T. D. Tilley, *J. Catal.*, 2005, **235**, 150–163.
24 K. L. Fujdala, I. J. Drake, A. T. Bell and T. D. Tilley, *J. Am. Chem. Soc.*, 2004, **126**, 10864–10866.
25 D. A. Ruddy, N. L. Ohler, A. T. Bell and T. D. Tilley, *J. Catal.*, 2006, **238**, 277–285.
26 P. J. Cordeiro, P. Guillo, C. S. Spanjers, J. W. Chang, M. I. Lipschutz, M. E. Fasulo, R. M. Rioux and T. D. Tilley, *ACS Catal.*, 2013, **3**, 2269–2279.
27 P. J. Cordeiro and T. D. Tilley, *Langmuir*, 2011, **27**, 6295–6304.
28 A. N. Bilyachenko, M. M. Levitsky, A. I. Yalymov, A. A. Korlyukov, V. N. Khrustalev, A. V. Vologzhanina, L. S. Shul'pina, N. S. Ikonnikov, A. E. Trigub, P. V. Dorovatovskii, X. Bantreil, F. Lamaty, J. Long, J. Larionova, I. E. Golub, E. S. Shubina and G. B. Shul'pin, *Angew. Chem. Int. Ed.*, 2016, **55**, 15360–15363.
29 R. D. Oldroyd, J. M. Thomas and G. Sankar, *Chem. Commun.*, 1997, 2025–2026.
30 R. D. Oldroyd, G. Sankar, J. M. Thomas and D. Özkaya, *J. Phys. Chem. B*, 1998, **102**, 1849–1855.
31 V. Cimpeanu, V. I. Parvulescu, P. Amorós, D. Beltrán, J. M. Thompson and C. Hardacre, *Chem. – Eur. J.*, 2004, **10**, 4640–4646.
32 C. M. Zicovich-Wilson and A. Corma, *J. Phys. Chem. B*, 2000, **104**, 4134–4140.
33 M. Moliner, M. J. Díaz-Cabañas, V. Fornés, C. Martínez and A. Corma, *J. Catal.*, 2008, **254**, 101–109.
34 J. M. Thomas, G. Sankar, M. C. Klunduk, M. P. Attfield, T. Maschmeyer, B. F. G. Johnson and R. G. Bell, *J. Phys. Chem. B*, 1999, **103**, 8809–8813.
35 P. Guillo, M. I. Lipschutz, M. E. Fasulo and T. D. Tilley, *ACS Catal.*, 2017, **7**, 2303–2312.
36 Y. Yamazaki, J. Přech, Y. Kuwahara, K. Mori, J. Čejka and H. Yamashita, *Catal. Today*, 2021, **376**, 28–35.
37 I. Mandache, V. I. Parvulescu, A. Popescu, L. Pârvulescu, M. D. Banciu, P. Amoros, D. Beltran, D. T. On and S. Kaliaguine, *Microporous Mesoporous Mater.*, 2005, **81**, 115–124.
38 E. Zeynep Ayla, D. Patel, A. Harris and D. W. Flaherty, *J. Catal.*, 2022, **411**, 167–176.
39 K. L. Fujdala and T. D. Tilley, *Chem. Mater.*, 2004, **16**, 1035–1047.
40 K. L. Fujdala and T. D. Tilley, *Z. Für Anorg. Allg. Chem.*, 2005, **631**, 2619–2622.
41 K. L. Fujdala, A. G. Oliver, F. J. Hollander and T. D. Tilley, *Inorg. Chem.*, 2003, **42**, 1140–1150.
42 J. P. Dombrowski, G. R. Johnson, A. T. Bell and T. D. Tilley, *Dalton Trans.*, 2016, **45**, 11025–11034.
43 J. W. Kriesel, M. S. Sander and T. D. Tilley, *Chem. Mater.*, 2001, **13**, 3554–3563.
44 J. W. Kriesel and T. D. Tilley, *J. Mater. Chem.*, 2001, **11**, 1081–1085.
45 M. P. Conley, M. F. Delley, G. Siddiqi, G. Lapadula, S. Norsic, V. Monteil, O. V. Safonova and C. Copéret, *Angew. Chem. Int. Ed.*, 2014, **53**, 1872–1876.
46 F. Allouche, G. Lapadula, G. Siddiqi, W. W. Lukens, O. Maury, B. Le Guennic, F. Pointillart, J. Dreiser, V. Mougel, O. Cador and C. Copéret, *ACS Cent. Sci.*, 2017, **3**, 244–249.
47 K. Searles, G. Siddiqi, O. V. Safonova and C. Copéret, *Chem. Sci.*, 2017, **8**, 2661–2666.
48 R. L. Brutchey, C. G. Lugmair, L. O. Schebaum and T. D. Tilley, *J. Catal.*, 2005, **229**, 72–81.
49 S. Yao, Y. Xiong and M. Driess, *Chem. – Eur. J.*, 2012, **18**, 11356–11361.
50 L. P. Stepovik and M. V. Gulenova, *Russ. J. Gen. Chem.*, 2006, **76**, 235–244.
51 Y. V. Fedotova, E. V. Zhezlova, T. G. Mushtina, A. N. Kornev, T. A. Chesnokova, G. K. Fukin, L. N. Zakharov and G. A. Domrachev, *Russ. Chem. Bull.*, 2003, **52**, 414–420.
52 H. F. Shurvell and M. C. Southby, *Vib. Spectrosc.*, 1997, **15**, 137–146.
53 Y. Abe and I. Kijima, *Bull. Chem. Soc. Jpn.*, 1969, **42**, 1118–1123.
54 D. A. Ruddy, J. Jarupatrakorn, R. M. Rioux, J. T. Miller, M. J. McMurdo, J. L. McBee, K. A. Tupper and T. D. Tilley, *Chem. Mater.*, 2008, **20**, 6517–6527.
55 R. L. Brutchey, D. A. Ruddy, L. K. Andersen and T. D. Tilley, *Langmuir*, 2005, **21**, 9576–9583.
56 D. Zhao, J. Feng, Q. Huo, N. Melosh, G. H. Fredrickson, B. F. Chmelka and G. D. Stucky, *Science*, 1998, **279**, 548–552.
57 M. Kruk, M. Jaroniec, C. H. Ko and R. Ryoo, *Chem. Mater.*, 2000, **12**, 1961–1968.
58 S. Vetrivel and A. Pandurangan, *J. Mol. Catal. Chem.*, 2006, **246**, 223–230.
59 I. Fechete, O. Ersen, F. Garin, L. Lazar and A. Rach, *Catal. Sci. Technol.*, 2013, **3**, 444–453.
60 R. Baran, L. Valentin and S. Dzwigaj, *Phys. Chem. Chem. Phys.*, 2016, **18**, 12050–12057.
61 Q. Zhang, Y. Wang, S. Itsuki, T. Shishido and K. Takehira, *J. Mol. Catal. Chem.*, 2002, **188**, 189–200.
62 N. Novak Tušar, S. Jank and R. Gläser, *ChemCatChem*, 2011, **3**, 254–269.
63 K. M. Parida, S. S. Dash and S. Singha, *Appl. Catal. Gen.*, 2008, **351**, 59–67.
64 M. Selvaraj, P. K. Sinha, K. Lee, I. Ahn, A. Pandurangan and T. G. Lee, *Microporous Mesoporous Mater.*, 2005, **78**, 139–149.
65 A. Ramanathan, T. Archipov, R. Maheswari, U. Hanefeld, E. Roduner and R. Gläser, *J. Phys. Chem. C*, 2008, **112**, 7468–7476.
66 Y. Meng, H. C. Genuino, C.-H. Kuo, H. Huang, S.-Y. Chen, L. Zhang, A. Rossi and S. L. Suib, *J. Am. Chem. Soc.*, 2013, **135**, 8594–8605.
67 A. Chakrabarti and I. E. Wachs, *Catal. Lett.*, 2015, **145**, 985–994.
68 A. Schweiger and G. Jeschke, *Principles of Pulse Electron Paramagnetic Resonance*, Oxford University Press, Oxford, New York, 2001.
69 R. Cammack and C. E. Cooper, *Methods Enzymol.*, 1993, **227**, 353–384.
70 M. P. Hendrich and P. G. Debrunner, *Biophys. J.*, 1989, **56**, 489–506.
71 W. R. Hagen, *Dalton Trans.*, 2006, **0**, 4415–4434.
72 S. K. Misra, S. Diehl, D. Tipikin and J. H. Freed, *J. Magn. Reson. San Diego Calif 1997*, 2010, **205**, 14–22.
73 D. G. Lonnon, G. E. Ball, I. Taylor, D. C. Craig and S. B. Colbran, *Inorg. Chem.*, 2009, **48**, 4863–4872.
74 W. R. Hagen, *Biochim. Biophys. Acta BBA - Protein Struct. Mol. Enzymol.*, 1982, **708**, 82–98.
75 D. Goldfarb, M. Bernardo, K. G. Strohmaier, D. E. W. Vaughan and H. Thomann, *J. Am. Chem. Soc.*, 1994, **116**, 6344–6353.
76 M. S. Kumar, M. Schwidder, W. Grünert and A. Brückner, *J. Catal.*, 2004, **227**, 384–397.
77 S. Bordiga, R. Buzzoni, F. Geobaldo, C. Lamberti, E. Giamello, A. Zecchina, G. Leofanti, G. Petrini, G. Tozzola and G. Vlaic, *J. Catal.*, 1996, **158**, 486–501.
78 B. M. Weckhuysen, D. Wang, M. P. Rosynek and J. H. Lunsford, *Angew. Chem. Int. Ed. Engl.*, 1997, **36**, 2374–2376.
79 V. Riollet, E. A. Quadrelli, C. Copéret, J.-M. Basset, R. A. Andersen, K. Köhler, R.-M. Böttcher and E. Herdtweck, *Chem. – Eur. J.*, 2005, **11**, 7358–7365.
80 J. S. Griffith, *Mol. Phys.*, 1964, **8**, 217–224.
81 C. G. Howard, G. S. Girolami, G. Wilkinson, M. Thornton-Pett and M. B. Hursthouse, *J. Chem. Soc. Dalton Trans.*, 1983, 2631–2637.

82 C. G. Howard, G. S. Girolami, G. Wilkinson, M. Thornton-Pett and M. B. Hursthouse, *J. Am. Chem. Soc.*, 1984, **106**, 2033–2040.
83 J. S. Griffith, *Mol. Phys.*, 1964, **8**, 213–216.
84 D. P. Goldberg, J. Telser, J. Krzystek, A. G. Montalban, L.-C. Brunel, A. G. M. Barrett and B. M. Hoffman, *J. Am. Chem. Soc.*, 1997, **119**, 8722–8723.
85 D. E. De Vos, B. M. Weckhuysen and T. Bein, *J. Am. Chem. Soc.*, 1996, **118**, 9615–9622.
86 A. Lita, X. Ma, R. W. Meulenberg, T. van Buuren and A. E. Stiegman, *Inorg. Chem.*, 2008, **47**, 7302–7308.
87 J. Krzystek, J.-H. Park, M. W. Meisel, M. A. Hitchman, H. Stratemeier, L.-C. Brunel and J. Telser, *Inorg. Chem.*, 2002, **41**, 4478–4487.
88 J. Krzystek, A. Ozarowski and J. Telser, *Coord. Chem. Rev.*, 2006, **250**, 2308–2324.
89 J. Telser, L. A. Pardi, J. Krzystek and L.-C. Brunel, *Inorg. Chem.*, 2000, **39**, 1834–1834.
90 D. G. Holah and J. P. Fackler, *Inorg. Chem.*, 1965, **4**, 1112–1116.
91 C. Dobe, C. Noble, G. Carver, P. L. W. Tregenna-Piggott, G. J. McIntyre, A.-L. Barra, A. Neels, S. Janssen and F. Juranyi, *J. Am. Chem. Soc.*, 2004, **126**, 16639–16652.
92 B. M. Weckhuysen, R. A. Schoonheydt, F. E. Mabbs and D. Collison, *J. Chem. Soc. Faraday Trans.*, 1996, **92**, 2431–2436.
93 B. V. Padlyak, J. Kornatowski, G. Zadrozna, M. Rozwadowski and A. Gutsze, *J. Phys. Chem. A*, 2000, **104**, 11837–11843.
94 M. F. Delley, F. Núñez-Zarur, M. P. Conley, A. Comas-Vives, G. Siddiqi, S. Norsic, V. Monteil, O. V. Safonova and C. Copéret, *Proc. Natl. Acad. Sci.*, 2014, **111**, 11624–11629.
95 F. L. Benedito, T. Petrenko, E. Bill, T. Weyhermüller and K. Wieghardt, *Inorg. Chem.*, 2009, **48**, 10913–10925.